

Estimation of Soil Electric Properties and Water Content Through PolSAR Target Decomposition

Mai Z. Ibrahim¹, Ahmed I. Bahnacy², Khalid F. A. Hussein³, and Asmaa E. Farahat³

¹High Institute of Electronic Engineering (HIEE)
High Institute of Electronic Engineering, Belbeis, Egypt
eng.mai695@gmail.com

²Department of Electronics and Communication Engineering
Faculty of Electronic Engineering, Menouf, 32952, Egypt
bahnacy@hotmail.com

³Microwave Engineering Department
Electronics Research Institute, Cairo, 11843, Egypt
fkhalid@eri.sci.eg, asmaa@eri.sci.eg

Abstract – A new method is proposed to recover the electric properties and water content of ground soil by applying the Target Decomposition (TD) theory for Polarimetric Synthetic Aperture Radar (PolSAR) images. The proposed method depends on the ε - σ characteristic curves of the soil which are unique for each soil type at a specific frequency. This method is examined for the clayey type soil which is found in most naturally vegetated land areas. Also, a novel method is developed for the realistic simulation of PolSAR images of natural lands, including forest regions, grasslands, and bare lands being prepared for gardens or crop cultivation. This method is based on the reverse of the PolSAR TD theory. The numerical results presented in this paper are concerned with the characterization of the most common type of clayey soil. Also, some of the numerical results presented in the present paper aim to achieve realistic PolSAR datasets using the inverse TD theory. Finally, some numerical results are presented for quantitative assessment of the method proposed to recover the properties and water content of the clayey soil using the datasets which are obtained through realistic simulations of forested areas, gardens, grasslands, and bare lands being prepared for cultivated plants. It is found, through the numerical investigations and quantitative assessment, that the dielectric constant, electric conductivity and water content of the investigated clayey types of soil are accurately estimated.

Index Terms – PolSAR, soil properties, target decomposition.

I. INTRODUCTION

The electric properties of the soil are of great importance in production agriculture. The dielectric constant and soil electric conductivity are measures of the amount of water content and salts in the soil. The soil's electric properties are important indicators of soil fertility and soil health. It affects crop yields, crop suitability, plant nutrient availability, and the activity of soil microorganisms, which influence key soil processes including the emission of greenhouse gases such as nitrogen oxides, methane, and carbon dioxide. For certain non-saline soils, determining the electric conductivity can be a convenient and economical way to estimate the amount of nitrogen available for plant growth [1].

In another field, many of the methods applied for the detection of buried landmines and unexploded ordnance make use of electromagnetic signals penetrating the land soil. The Ground-Penetrating Radar (GPR) is considered the most promising technology for this purpose because of its ability to detect both metallic and non-metallic anti-personnel landmines by non-invasive subsurface sensing. However, the electric properties of the soil medium are critical parameters for buried object detection using the GPR because they control the contrast between the buried object and the soil in which it is buried. Additionally the electric properties of the soil control propagation, attenuation, and reflection of electromagnetic waves. Under some soil conditions, the landmine signature is of high quality while under others no signature can be detected at all [2].

Soil moisture is the quantity of water contained in soil on a volumetric or gravimetric basis [3, 4].

Soil moisture influences meteorological and climatic processes, although surface soil moisture only constitutes 0.0012% of all water available on the earth [5]. Soil moisture is important in modeling the ecosystem dynamics and the biogeochemical cycles but it has not had widespread application in modeling these processes because it is a variable that is very difficult to measure a spatially comprehensive basis [6]. The soil moisture gives also important information for agriculture irrigation. An accurate estimate of the spatiotemporal variations of soil moisture is critical for numerous large-scale environmental studies [7]. The large spatial and temporal variability that soil water content exhibit in the natural environment is the characteristic that makes it difficult to measure and use in earth science applications.

The use of radar data to retrieve soil moisture is of considerable importance in many domains, including agriculture, hydrology, and meteorology [6]. Despite many advantages that can be derived from the knowledge of soil moisture distribution, the measurement of soil moisture has a few limitations. However, the measurement of soil moisture not only depends on target characteristics such as surface roughness, vegetation cover, dielectric constant, and topography but also depends on various combinations of the radar sensor parameters including frequency, polarization, and angle of incidence (θ) with respect to nadir [9]. The measurements depend on the separation of the effects of water content and other factors such as surface roughness or soil texture which affect the backscattered signal. Unfortunately, most of the studies deal with the relationships obtained between the backscattering coefficient and soil moisture for a given set of radar configuration parameters. In [9], the soil moisture is estimated approximately from the microwave backscattering coefficients for the case of bare soil. In [10], soil surface parameters are retrieved from fully polarimetric SAR data.

Polarimetric Target Decomposition (TD) enables the physical interpretation of synthetic aperture radar (SAR) images more easily by fitting physical models of electromagnetic scattering to the PolSAR observations [11].

The theory of TD formulates the total scattering from a ground target as the sum of elementary scattering mechanisms to interpret the scattering from a land target as the weighted contributions of multiple physical mechanisms. This facilitates the identification, recognition, and classification of possible land targets with distinguishing polarization features.

In this paper, a novel method is applied to estimate the electric properties and the water content of ground soil using the TD theorem and the ϵ - σ characteristic curves of the soil which are unique for each soil type at a specific frequency. The proposed method is examined for clayey soil found in most naturally vegetated land

areas. Also, a novel method is developed in the present paper for realistic simulation of PolSAR images for natural lands including forest regions, grasslands, and bare lands being prepared for gardens or crop cultivation. This method is based on the reverse of the PolSAR TD theory. The numerical results presented in this paper are concerned with the characterization of the clayey soil found in most of the natural lands, especially the vegetal regions. Also, some numerical results are presented to get datasets for a novel technique that is proposed for the realistic simulation of PolSAR images. Finally, some numerical results are presented for quantitative assessment of the method proposed for the estimation of the electric properties and water content of the clayey soil found in the forested areas, gardens, grasslands, and bare lands being prepared for cultivated plants.

II. ELECTRIC PROPERTIES OF THE GROUND SOIL OF CLAYEY TYPE

Clayey soil is the most common type of ground soils found in vegetal natural lands such as the natural grasslands, forest regions, and the soils prepared for cultivated crops. Clay is a type of fine-grained natural soil material that contains hydrous aluminum phyllosilicates (clay minerals) that develops plasticity when wet. Geologic clay deposits are mostly composed of phyllosilicate minerals containing variable amounts of water trapped in the mineral structure. Clays are plastic due to particle size and geometry as well as water content and become hard, brittle, and non-plastic upon drying or firing. Water does not percolate quickly enough through clayey soil. The water needs a relatively long time to soak into the earth. If the clayey soil is watered too much all at once, water just runs off and is wasted. Moreover, the clayey soil types retain water well and, hence, should be watered less frequently. The excess water should be gotten away otherwise the plants' roots are drowned.

The dielectric constant of the ground soil (ϵ_g) is complex and can be given as follows:

$$\epsilon_g = \epsilon_{rg} - j\epsilon_{ig}. \quad (1-a)$$

The imaginary part of the relative permittivity is expressed in terms of the soil conductivity, σ_g , as follows:

$$\epsilon_{ig} = \frac{\sigma_g}{2\pi f \epsilon_0}. \quad (1-b)$$

The electric properties of the most common types of ground soils are dispersive with the frequency. It has its complex dielectric constant varying with the frequency. The electric properties of the soil are, also, strongly dependent on its volumetric water content and the continuous change of the soil water content leads to simultaneous continuous and monotonic variations of real dielectric constant, ϵ_{rg} , and conductivity, σ_g [12]. At any microwave frequency, the two electric properties ϵ_{rg} and σ_g are strongly correlated, which allows

a mathematical relation between them to be calculated. This enables the expression of σ_g as a single-valued function of ϵ_{rg} as follows:

$$\sigma_g = F(\epsilon_{rg}). \quad (2)$$

Given a microwave frequency, the ϵ - σ characteristic curve expressed in (2) is unique for each type of soil and provides important information that describes the relationship between the real dielectric constant, ϵ_{rg} , and the electric conductivity, σ_g , at the frequency of operation. These characteristic curves have great importance for the recovery of the electric properties and water content of the soil using the technique introduced in this work.

III. POLSAR TARGET DECOMPOSITION FOR ESTIMATION OF SOIL PROPERTIES AND WATER CONTENT

The covariance matrix of the PolSAR data is given by (A.1) of the Appendix. This covariance matrix is normalized, as given in (A.7) of the Appendix, and it has a unity ratio of the backscattered power, i.e. the summation of its main diagonal elements is equal to 1; hence:

$$\hat{\sigma}_p^2 = \hat{\sigma}_{hh}^2 + 2\hat{\sigma}_{hv}^2 + \hat{\sigma}_{vv}^2 = 1. \quad (3)$$

The PolSAR target decomposition theory with five-component scattering model [13] can be applied to get the following expansion of $\hat{\Sigma}$:

$$\hat{\Sigma} = a_s \hat{C}_s + a_d \hat{C}_d + a_v \hat{C}_v + a_w \hat{C}_w + a_h \hat{C}_h, \quad (4)$$

where \hat{C}_s , \hat{C}_d , \hat{C}_v , \hat{C}_w , and \hat{C}_h are the normalized basis covariance matrices used to decompose $\hat{\Sigma}$ and represent the basic scattering mechanisms due to single bounce of the incident wave on the rough soil surface, double-bounce on right-angle corners, volume scattering, wire (edge) scattering, and helix scattering. The expressions of these matrices are supplied in the appendix.

In the present analysis, due to the use of normalized covariance matrices on both sides of (4), the power balance implies that the coefficients a_s , a_d , a_v , a_w , and a_h are real unknown coefficients and, also, requires:

$$a_s + a_d + a_v + a_w + a_h = 1. \quad (5)$$

The contributions of wire and helix scattering mechanisms to the PolSAR data result from the human made structures which are usually found in urban areas. Such constituents are not found in natural lands such as forested regions grasslands, bare (unplanted) soil areas, deserts, sea surfaces, etc. Under this consideration, one can set $a_h = a_e = 0$ in (5). Thus, the decomposition of the normalized covariance matrix of the PolSAR data collected for the ground regions with natural land covers can be achieved using the following scattering model that is based on the three natural scattering components:

$$\hat{\Sigma} = a_s \hat{C}_s + a_d \hat{C}_d + a_v \hat{C}_v, \quad (6-a)$$

with the following condition which is necessary for power balance:

$$a_s + a_d + a_v = 1. \quad (6-b)$$

Using the expressions of the normalized basis covariance matrices \hat{C}_s , \hat{C}_d , and \hat{C}_v , supplied in the appendix, the application of (6) results in the following system of equations:

$$\hat{\sigma}_{hh}^2 = \frac{|\beta|^2}{1+|\beta|^2} a_s + \frac{|\alpha|^2}{1+|\alpha|^2} a_d + \frac{3}{8} a_v, \quad (7-a)$$

$$2\hat{\sigma}_{hv}^2 = \frac{1}{4} a_v, \quad (7-b)$$

$$\hat{\sigma}_{vv}^2 = \frac{1}{1+|\beta|^2} a_s + \frac{1}{1+|\alpha|^2} a_d + \frac{3}{8} a_v, \quad (7-c)$$

$$\hat{\sigma}_{hh,vv}^2 = \frac{\beta}{1+|\beta|^2} a_s + \frac{\alpha}{1+|\alpha|^2} a_d + \frac{1}{8} a_v, \quad (7-d)$$

where the expression for α and β supplied in the appendix. Considering that $\alpha = \alpha_r + j\alpha_i$ and $\beta = \beta_r + j\beta_i$, the nonlinear system of equations (7) can, generally, be seen as composed of five real equations in seven real unknowns (a_s , a_d , a_v , α_r , α_i , β_r , and β_i). Thus, the solution of such a system may result in an infinite number of possible and acceptable solutions unless other constraints related to the ground soil properties are imposed to get the correct solution for the seven unknowns.

IV. THE PROPOSED METHOD FOR ESTIMATION OF SOIL PROPERTIES AND WATER CONTENT

The most common three types of natural lands (see Fig. 1) are investigated in the present work: the forest regions, grasslands, and bare soils. The forest regions need a three-component scattering model for the decomposition of the covariance matrix as the contribution of the single-bounce, double-bounce, and volume scattering should all be considered in the PolSAR data. The grasslands need a two-component scattering model due to the contributions of the single-bounce and volume scattering. The bare soils need a single-component scattering model as only the single bounce of the incident wave on the rough soil surface of the bare land constitutes the SAR data.

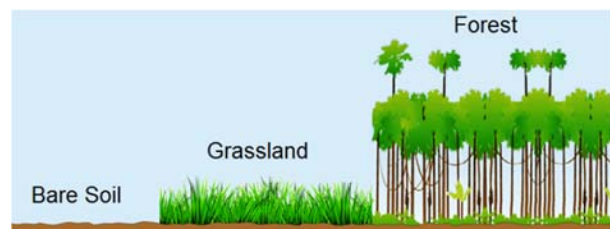


Fig. 1. The most common types of natural ground: Bare soils, grasslands, and forest regions.

Parameter β , appearing in (7), is related to the single bounce of the incident wave on the rough surface of the ground soil. As given in the appendix, for a given

look angle (θ_i) of the SAR, this parameter is uniquely determined by the complex relative permittivity of the soil (ϵ_{rg}, σ_g). On the other hand, the parameter α , appearing in (7), is related to the double-bounce of the incident wave on the right-angle corners formed by the horizontal surface of the ground soil and the vertical surface of the tree trunks. As given in the appendix, for a given look angle (θ_i), this parameter depends on the complex relative permittivity of the soil and that of the tree trunks. The complex dielectric constant of a tree trunk measured at the trunk surface is usually constant for a specific frequency and is weakly dependent on the water content of the tree [14]. Thus, for a specific tree type, the parameter α is strongly dependent on the complex relative permittivity of the ground soil (ϵ_{rg}, σ_g). As the electric parameters (ϵ_{rg}, σ_g) of a ground soil of a specific type are determined by its water content, parameters α and β can be uniquely determined by the water content of the ground soil beneath the vegetation.

A. Estimation of electric properties and water content of the ground soil of forest regions

Regarding the decomposition of $\hat{\Sigma}$ given by (6) for all types of natural land covers, it should be considered, for the forest regions, that $a_s \neq 0$ due to the significant contribution of the single bounce of the incident wave on the rough soil surface beneath the forest trees, $a_d \neq 0$ due to strong contribution of double-bounce on the right-angle corners formed by the horizontal ground surface and vertical tree trunks, and $a_v \neq 0$ due to the volume scattering from the huge tree canopy layer. Thus, the three components of backscattering are all present in the PolSAR data of the forest regions.

Considering $a_v = 8 \hat{\sigma}_{hv}^2$ as given by (7-b), the system of equations given by (7) can be reduced to take the following form:

$$a_s + a_d = 1 - 8\hat{\sigma}_{hv}^2, \quad (8-a)$$

$$\frac{1-|\beta|^2}{1+|\beta|^2} a_s + \frac{1-|\alpha|^2}{1+|\alpha|^2} a_d = \hat{\sigma}_{vv}^2 - \hat{\sigma}_{hh}^2, \quad (8-b)$$

$$\frac{\beta}{1+|\beta|^2} a_s + \frac{\alpha}{1+|\alpha|^2} a_d = \hat{\sigma}_{hh,vv}^2 - \hat{\sigma}_{hv}^2. \quad (8-c)$$

In this case, the system (8) can be seen as composed of four real equations and six real unknowns ($a_s, a_d, \alpha_r, \alpha_i, \beta_r, \beta_i$). It seems that, unless other constraints are imposed, the system given by (8) cannot have a unique solution. Using (8-a) and (8-b), the coefficients a_s and a_d can be obtained in terms of the other complex unknowns α and β as follows:

$$a_s = 1 - 8\hat{\sigma}_{hv}^2 - \frac{\hat{\sigma}_{vv}^2 - \hat{\sigma}_{hh}^2 - \frac{1-|\beta|^2}{1+|\beta|^2} (1 - 8\hat{\sigma}_{hv}^2)}{\frac{1-|\alpha|^2}{1+|\alpha|^2} - \frac{1-|\beta|^2}{1+|\beta|^2}}, \quad (9-a)$$

$$a_d = \frac{\hat{\sigma}_{vv}^2 - \hat{\sigma}_{hh}^2 - \frac{1-|\beta|^2}{1+|\beta|^2} (1 - 8\hat{\sigma}_{hv}^2)}{\frac{1-|\alpha|^2}{1+|\alpha|^2} - \frac{1-|\beta|^2}{1+|\beta|^2}}. \quad (9-b)$$

A third complex equation can be formulated as a quantity δ_F being equal to the difference between the left-hand and right-hand sides of (8-c), where:

$$\delta_F = \frac{\beta}{1+|\beta|^2} a_s + \frac{\alpha}{1+|\alpha|^2} a_d - (\hat{\sigma}_{hh,vv}^2 - \hat{\sigma}_{hv}^2). \quad (10)$$

The coefficients a_s and a_d can be substituted from (9) into (10) to get δ_F completely expressed in terms of α and β which are uniquely determined by ϵ_{rg} and σ_g as given by (A.9) and (A.10), respectively. In this way, the problem is formulated as follows: Find the values of ϵ_{rg} and σ_g to get $\delta_F = 0$. Thus, a complex equation given by (1) in two real unknowns (ϵ_{rg} and σ_g) is formulated. A constraint on the relation between the two unknowns is given by the ϵ - σ characteristic curve, expressed in (2), that uniquely characterizes the soil beneath the vegetation. In this way, a unique solution for ϵ_{rg} and σ_g can be obtained by minimizing δ_F given by (10), and, then, the ϵ - σ characteristic curve can be used to uniquely determine the water content of the soil. Also, the parameters α and β can be calculated using (A.9) and (A.10), respectively, and substituted into (9) to get the unknown coefficients a_s and a_d . Thus, the contribution of each of the three scattering mechanisms is determined by the triplet (a_s, a_d, a_v) and, hence, the imaged land is classified.

B. Estimation of electric properties and water content of the ground soil of grasslands

Regarding the expansion of $\hat{\Sigma}$ given by (6) for natural land covers, it should be considered, for the grasslands, that $a_s \neq 0$ due to the significant contribution of the single bounce of the incident wave on the rough soil surface beneath the grass leaves, $a_d = 0$ due to absence of double-bounce, and $a_v \neq 0$ due to the volume scattering from the dense leaves of the grass. Thus, for grasslands, the normalized covariance matrix $\hat{\Sigma}$ has only two components of scattering and can be decomposed as follows:

$$\hat{\Sigma} = a_s \hat{C}_s + a_v \hat{C}_v. \quad (11)$$

For grown grasslands, $a_s \neq 0$ and $a_v \neq 0$ and, hence, the application of (11) results in the following system of equations:

$$a_v = 8\hat{\sigma}_{hv}^2, \quad (12-a)$$

$$a_s = 1 - 8\hat{\sigma}_{hv}^2, \quad (12-b)$$

$$\frac{1-|\beta|^2}{1+|\beta|^2} (1 - 8\hat{\sigma}_{hv}^2) = \hat{\sigma}_{vv}^2 - \hat{\sigma}_{hh}^2, \quad (12-c)$$

$$\frac{\beta}{1+|\beta|^2} (1 - 8\hat{\sigma}_{hv}^2) = \hat{\sigma}_{hh,vv}^2 - \hat{\sigma}_{hv}^2. \quad (12-d)$$

Equation (12-c) can be rearranged and written in the following form:

$$1 + |\beta|^2 = \frac{2(1 - 8\hat{\sigma}_{hv}^2)}{1 - 8\hat{\sigma}_{hv}^2 + \hat{\sigma}_{vv}^2 - \hat{\sigma}_{hh}^2}. \quad (13)$$

The substitution from (13) into (12-d) gives the following solution for β :

$$\beta = \frac{2(\hat{\sigma}_{hh,vv}^2 - \hat{\sigma}_{hv}^2)}{1 - 8\hat{\sigma}_{hv}^2 + \hat{\sigma}_{vv}^2 - \hat{\sigma}_{hh}^2}. \quad (14)$$

A complex equation can be formulated as a quantity δ_G being equal to the difference between the left-hand and right-hand sides of (12-d), where,

$$\delta_G = \frac{\beta}{1 + |\beta|^2} (1 - 8\hat{\sigma}_{hv}^2) - (\hat{\sigma}_{hh,vv}^2 - \hat{\sigma}_{hv}^2). \quad (15)$$

The equation $\delta_G = 0$ has a unique solution for ε_{rg} and σ_g and the corresponding water content can, then, be directly determined from the ε - σ characteristic curve of the specified type of the grassland soil. On the other hand, the contributions of the single-bounce and volume scattering mechanisms to $\hat{\Sigma}$ is determined by the doublet (a_s, a_d) and, hence, the imaged land is classified.

C. Estimation of electric properties and water content of bare soil

Regarding the expansion of $\hat{\Sigma}$ given by (6), it should be considered that, for the bare soil regions, only $a_s \neq 0$ due to the contribution of the single bounce of the incident wave on the rough soil surface. For the other two coefficients, one has $a_d = 0$ and $a_v = 0$ due to the absence of double-bounce and vegetation canopies, respectively. Thus, for bare soil areas, the normalized covariance matrix $\hat{\Sigma}$ can be expressed as follows.

$$\hat{\Sigma} = a_s \hat{C}_s. \quad (16)$$

As the covariance matrices on both sides of (16) are normalized, the following system of equations is obtained:

$$a_s = 1, \quad (17-a)$$

$$\frac{|\beta|^2}{1 + |\beta|^2} = \hat{\sigma}_{hh}^2, \quad (17-b)$$

$$\frac{\beta}{1 + |\beta|^2} = \hat{\sigma}_{hh,vv}^2. \quad (17-c)$$

Equation (17-b) can be rearranged and written in the following form:

$$1 + |\beta|^2 = \frac{1}{1 - \hat{\sigma}_{hh}^2}. \quad (18)$$

By substitution from (18) into (17-c) gives the following solution for β :

$$\beta = \frac{\hat{\sigma}_{hh,vv}^2}{1 - \hat{\sigma}_{hh}^2}. \quad (19)$$

A complex equation can be formulated as a quantity δ_S being equal to the difference between the left-hand and right-hand sides of (17-c), where:

$$\delta_S = \frac{\beta}{1 + |\beta|^2} - \hat{\sigma}_{hh,vv}^2. \quad (20)$$

The equation $\delta_S = 0$ has a unique solution for ε_{rg} and σ_g ; then the corresponding water content can directly be determined from the ε - σ characteristic curve of the specified type of the bare soil.

V. SIMULATION OF POLSAR IMAGES OF NATURAL LANDS

PolSAR datasets (test images) are required for testing the efficiency of the technique proposed in the present work for the classification of natural lands of clayey soil and estimation of water content. The natural lands investigated include forest regions, natural grasslands, and bare soils. Such datasets can be obtained by simulation. It is proposed to apply the target decomposition theory with the three-component scattering model as described in Section III to construct a covariance matrix that describes the statistical properties of the PolSAR data collected upon imaging the desired area of the natural land. The detailed procedure to generate a realistic PolSAR image can be described as follows.

- The texture (composition of ingredients) of the ground soil should be specified.
- The curves describing the relations between the electromagnetic properties of the ground soil type (with the texture specified in the previous step) and the water content should be known.
- The ε - σ characteristic curves of the soil at the PolSAR operating frequency should be known.
- The volumetric water content w_{ref} of the ground soil and the corresponding electric properties $\varepsilon_{g,ref}$ and $\sigma_{g,ref}$ should be determined.
- The azimuth and range dimensions of the land area to be imaged (by simulation), L_A and L_R , should be given.
- The desired azimuth and range resolutions ρ_A and ρ_R , of the simulated PolSAR image should be given.
- Parameters α_{ref} and β_{ref} are evaluated by (A.9) and (A.10) as given in the appendix. For the forest regions, the electric properties of the tree trunks should be known (or assumed) to calculate α_{ref} .
- The normalized basis covariance matrices \hat{C}_s , \hat{C}_d , and \hat{C}_v are evaluated using (A.8-a), (A.8-b), and (A.8-c) as given in the appendix.
- The desired contributions of the three scattering mechanisms $a_{s,ref}$, $a_{d,ref}$, and $a_{v,ref}$ are determined according to actual constituents of the imaged land.
- A normalized covariance matrix, $\hat{\Sigma}_{ref}$, is constructed by composition using the three-component scattering model given by (6) for the type of natural land.
- The desired level of the backscattered power to the power illuminating the SAR target (imaged land area), P_{ref} , should be determined.

- The covariance matrix is calculated, $\Sigma_{ref} = P_{ref} \hat{\Sigma}_{ref}$.
- The dimensions (size) of the simulated PolSAR image in the azimuth and range directions are obtained as $M = L_A/\rho_A$ and $N = L_R/\rho_R$, respectively.
- Finally, the covariance matrix Σ_{ref} is used to generate a simulated three-channel image of $M \times N$ pixels defined by $S_{m,n} = \{S_{hh}, S_{hv}, S_{vv}\}_{m,n}$.

VI. RESULTS AND DISCUSSIONS

This section presents the numerical results concerned with, (i) Characterization of the clayey soil found in most of the natural lands, especially the vegetal regions. (ii) Application of the method proposed in Section V that uses the theory of SAR target decomposition for realistic simulation of PolSAR images. (iii) Application of the method proposed in Section IV for estimation of the electric properties and water content of the clayey soil found in the forested areas, gardens, grasslands, and bare lands being prepared to cultivate plants.

A. Texture of the clayey soil commonly found in natural lands

The clayey types of soil investigated in the present work are characterized in [12] through experimental measurements. The ingredients and volumetric density of this type of soil are listed in Table 1. This is the most common type of ground soil found in natural lands such as natural grasslands, forest regions, and the bare soils being prepared for cultivated crops.

Table 1: Composition of the clayey soil type used for testing the method introduced in the present work to estimate the soil properties [12]

Soil Type	Soil Composition (%)			Bulk Density (gm/cm^3)
	Sand	Slit	Clay	
Clayey	17.25	39.04	43.05	1.2

B. Dispersive electric properties and $\varepsilon - \sigma$ characteristic curves of the clayey soil

Clayey soil with the composite texture listed in Table 1 and 30% water content has its complex dielectric constant varying with the frequency as shown in Fig. 2 (a) [12]. The electric properties of this soil are also strongly dependent on its volumetric water content. The PolSAR systems used for vegetation monitoring usually operate at 1.27 GHz. For the clayey soil with the texture listed in Table 1, the curves describing the dependence of ε_{rg} and ε_{ig} on the volumetric water content at 1.27 GHz are deduced from those available in [12] at 900 MHz by

the aid of the frequency dispersion curves presented in Fig. 2 (a). The curves describing the dependence of ε_{rg} and σ_g on the water content at 900 MHz and 1.27 GHz are presented in Fig. 2 (b). The continuous change of the soil water content leads to simultaneous continuous monotonic variations of its electric properties as shown in Fig. 2 (b). At any microwave frequency, the electric properties ε_{rg} , and σ_g are strongly correlated and, hence, a curve can be fitted between them as previously mentioned in Section II.

C. Realistic simulation of PolSAR datasets for natural lands

PolSAR datasets (test images) are required to test the methods introduced in the present work for the classification of natural lands of clayey soil and estimation of water content. The procedure described in Section V is applied to generate three datasets for the three types of natural lands investigated in this work.

For the simulated PolSAR images, it is considered that the working frequency is 1.27 GHz and the ground soil is clayey with the mixture of ingredients listed in Table 1. The ground soil has the $\varepsilon - \sigma$ characteristic curves presented in Fig. 2 (c), the water content is 44% and the corresponding electric properties are $\varepsilon_{rg.ref} = 25.16$ and $\sigma_{g.ref} = 0.489 S/m$. The electric properties of the tree trunks are $\varepsilon_{rw} = 4$, and $\sigma_w = 0.01 S/m$. The corresponding values of α and β , given by (A.9) and (A.10), respectively, are $\alpha_{ref} = 4.7091 - j0.2981$, and $\beta_{ref} = 0.4073 + j0.0132$. Using these values, the normalized basis covariance matrices for the single-bounce, \hat{C}_s , double-bounce, \hat{C}_d , and volume scattering, \hat{C}_v , mechanisms can be calculated using (A.8-a), (A.8-b), and (A.8-c).

C.1. Covariance matrix for PolSAR images of forested areas

Consider a forested area with equal contributions of the three basic constituents (single-bounce, double-bounce, and volume scattering) to the backscatter data collected by a PolSAR system, i.e., $a_s = a_d = a_v = 1/3$. Considering that this forested area has a clayey soil of water content of 44%, the application of (6) with the obtained normalized covariance matrices, \hat{C}_s , \hat{C}_d , and \hat{C}_v , the normalized covariance matrix, $\hat{\Sigma}_{F.ref}$, for the three-channel PolSAR image data of this forest region can be calculated.

C.2. Covariance matrix for PolSAR images of grasslands

Consider a grassland area for which the contribution of the double-bounce to the PolSAR data vanishes whereas the volume scattering caused by the grass leaves is twice that of the single-bounce scattering caused by the soil rough surface, i.e., $a_s = 1/3$, $a_d = 0$, and $a_v = 2/3$.

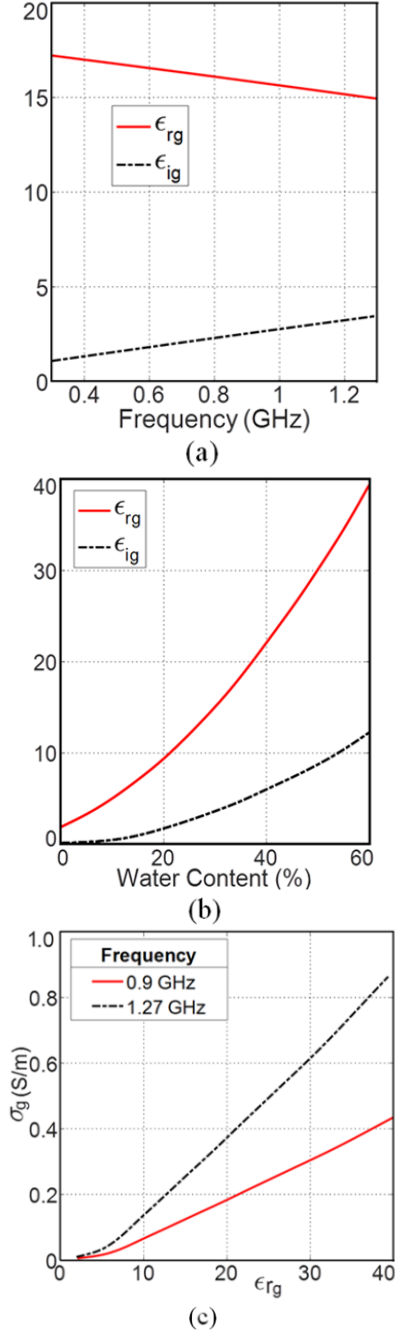


Fig. 2. Dependence of the complex relative permittivity of the clayey soil on the frequency and volumetric water content. (a) Dispersive properties at 30% water content, (b) Dependence of ϵ_{rg} and σ_g on the water content, (c) ϵ - σ characteristic curves.

Considering that this grassland area has a clayey soil of water content of 44%, the application of (6) with the obtained normalized covariance matrices \hat{C}_s , \hat{C}_d , and \hat{C}_v , the normalized covariance matrix, $\hat{\Sigma}_{Fref}$, for the three-channel PolSAR image data of this grassland.

C.3. Covariance matrix for PolSAR images of bare soil areas

An area of bare clayey soil with 44% water content has its backscattering attributed only to the single-bounce mechanism and, hence, the normalized covariance matrix for the three-channel PolSAR image data can be given directly as $\hat{\Sigma}_{Sref} = \hat{C}_s$.

C.4. Simulated PolSAR Images

C.4.1. Ground truth images of natural lands with clayey soil

To visualize the classified natural lands by monitoring the water content of the ground soil, a color map may be appropriate for this purpose. The RGB colors used for indicating the three basic scattering mechanisms in the natural land of the clayey soil described in Section VI-A, single-bounce, double-bounce, and volume scattering are, respectively, expressed as follows:

$$RGB_{SB} = (0.6, 0.6, 0.4), \quad (21-a)$$

$$RGB_{DB} = (0.8, 0.2, 0.0), \quad (21-b)$$

$$RGB_{VS} = (0.2, 0.6, 0.2). \quad (21-c)$$

The RGB colors used to indicate the type of the natural land while monitoring the water content of the soil can generally be composed as follows:

$$RGB_{NaturalLand} = (a_s RGB_{SB} + a_d RGB_{DB} + a_v RGB_{VS}) (1-w)^{0.7}, \quad (22)$$

where w is the volumetric water content. For example, the RGB color codes for the pure land types (forest, grasslands, and bare lands) of clayey soils are, respectively expressed as follows:

$$RGB_{Forest} = \left(\frac{1}{3} RGB_{SB} + \frac{1}{3} RGB_{DB} + \frac{1}{3} RGB_{VS} \right) (1-w)^{0.7}, \quad (23-a)$$

$$RGB_{GrassLand} = \left(\frac{1}{3} RGB_{SB} + \frac{2}{3} RGB_{VS} \right) (1-w)^{0.7}, \quad (23-b)$$

$$RGB_{BareLand} = RGB_{SB} (1-w)^{0.7}. \quad (23-c)$$

The color map shown in Fig. 3 is appropriate for simultaneous monitoring of the natural land type and the water content of the ground soil beneath the vegetation.

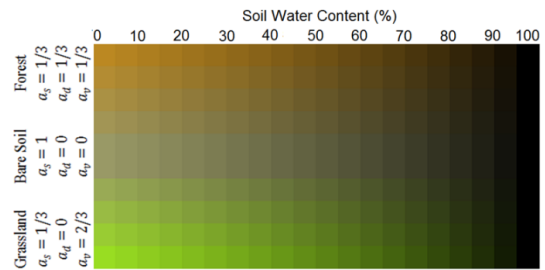


Fig. 3. Color map for classification of the natural lands with indication of the soil water content.










The RGB colors shown in this figure are generated using (23). For all the types of natural lands, the darkness of the corresponding color indicates the water content of the ground soil.

C.4.2. Simulated PolSAR Images for Natural Lands

An optical satellite image obtained from Google Maps for a region of cultivated land near Luxor Luxury Villa, in Luxor city, Egypt, is presented in Fig. 4 (a). A corresponding image is presented in Fig. 4 (b) to classify the different types of natural lands with the color code listed Table 2. The total dimensions of the land region to be imaged in the azimuth and range directions are $L_A = 365\text{ m}$ and $L_R = 400\text{ m}$, respectively.

The procedure described in Section V is applied to get the three-channel PolSAR images, where the corresponding resolutions are set as $\rho_A = 0.65\text{ m}$ and $\rho_R = 0.71\text{ m}$, respectively. Thus, the size of the simulated PolSAR image is 560×565 pixels in the azimuth and range directions, respectively. A ground-truth image is presented in Fig. 5 (a) to indicate the land type by monitoring the soil water content according to the color map shown in Fig. 3. The generated three-channel PolSAR images are presented in Figs. 5 (b), (c), and (d). The image of the cross-polarization HV-channel, $|S_{hv}|$, Fig. 5 (c), shows a high level of the cross-polarized backscatter from the vegetal areas (forests and grasslands) whereas the water surface and bare lands have almost zero cross-polarization. Also, for the regions characterized by single-bounce scattering like water surface and bare land, the backscatter of the co-polarization VV-channel, $|S_{vv}|$, is significantly larger than $|S_{hh}|$, of the HH-channel.

Table 2: Color code for classification of natural land types included in the imaged region presented in Fig. 4

Color code	Type of natural land	Soil water content	Dielectric constant	Electric conductivity (S/m)
 Forest 1	Forested area	19 %	8.907	0.1109
 Forest 2	Forested area	29 %	14.45	0.2416
 Forest 3	Forested area	44 %	25.16	0.4980
 Forest 4	Forested area	54 %	33.56	0.7067
 Grassland 1	Grassland	25 %	12.10	0.1860
 Grassland 2	Grassland	39 %	21.33	0.4060
 Grassland 3	Grassland	49 %	29.22	0.5958
 Bare Land 1	Bare land	34 %	17.68	0.3172
 Bare Land 2	Bare land	56 %	35.40	0.7567

D. Estimation of electric properties of clayey soil in natural lands

The proposed method is used to estimate the electric properties of different soil types.

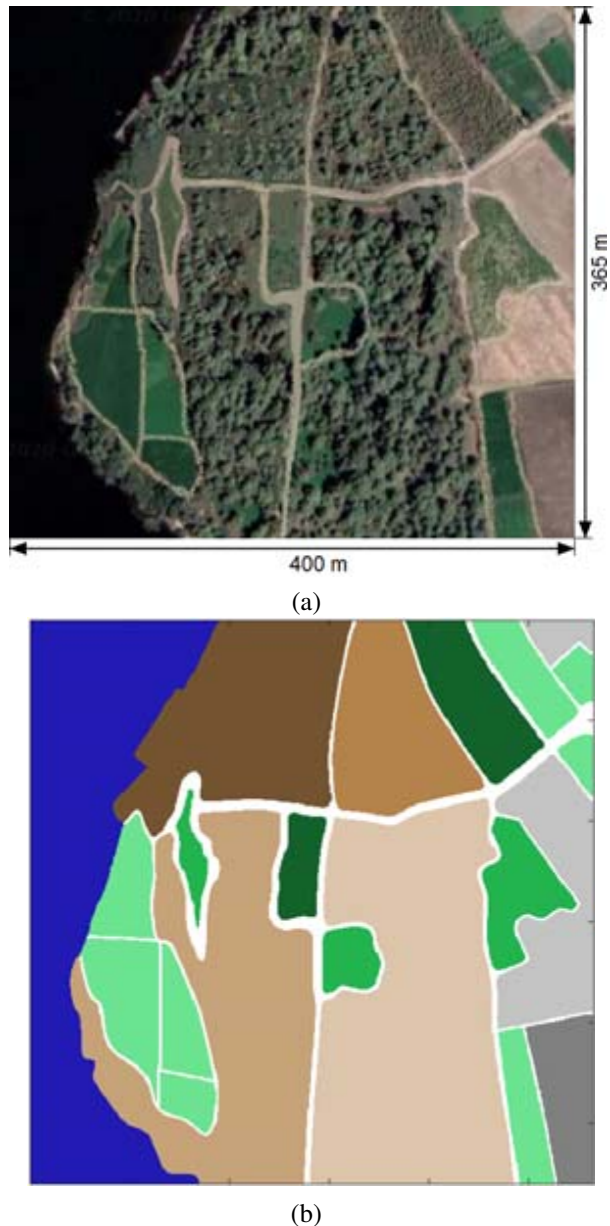


Fig. 4. Region of cultivated land near Luxor Luxury Villa, in Luxor city, Egypt, (a) satellite image obtained from Google Maps, (b) Color-coded classification image according to the type of land; Table 2 for legend.

D.1. Estimation of electric properties of clayey soil in forest regions

The method described in Section IV-A is used to estimate the properties of the ground soil of the forested area named “Forest 3”, see Fig. 4, from the corresponding PolSAR data presented in Figs. 5 (b), (c), (d) with the ground truth shown in Fig. 5 (a).

The quantity δ_F , expressed in (10), is plotted as a function of ϵ_{rg} and σ_g in a three-dimensional plot as

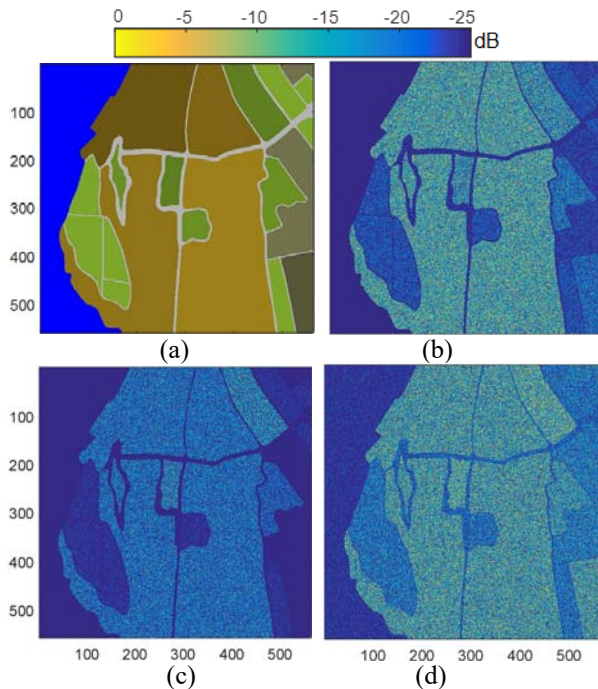


Fig. 5. Simulation of three-channel PolSAR image for the land region in Luxor city, (a) Ground-truth image showing the land type with indication of the soil water content, (b) $|S_{hh}|$, (c) $|S_{hv}|$, (d) $|S_{vv}|$, channels.

shown in Fig. 6. The ϵ - σ characteristic curve of the soil is also plotted in the $(\epsilon_{rg}-\sigma_g)$ plane of Fig. 6. It is shown that δ_F has a sharp minimum of 8×10^{-5} at the point $\epsilon_{rg} = 25.2$ and $\sigma_g = 0.519 S/m$, which almost lies on the ϵ - σ characteristic curve of the clayey soil as shown in Fig. 6, where the corresponding water content of the soil is 44.57%. The estimated values of the electric properties, ϵ_{rg} and σ_g , and the water content are listed in Table 3 with the resulting estimation errors. It is found that the percentage estimation errors are very small which reflects the efficiency of the proposed method to estimate the electric properties and water content of the soil using.

Table 3: The ground soil parameters used for generating the SAR data for the forested area named “Forest 3”; see Table 2. The estimated values of these parameters using the proposed method and the resulting estimation errors are listed in the last two rows of the table

Soil Parameter	Dielectric Constant ϵ_{rg}	Conductivity (S/m) σ_g	Water Content w
Ground Truth	25.16	0.498	44.00 %
Estimated	25.20	0.519	44.57 %
Percentage Error	0.16 %	4.1 %	1.3 %

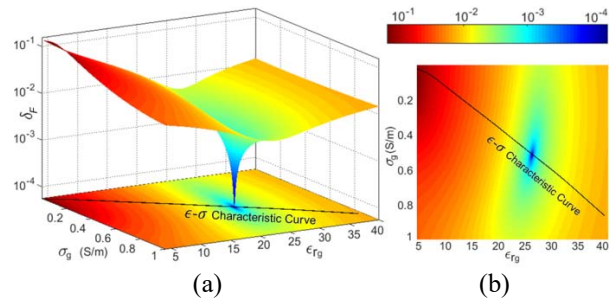


Fig. 6. Estimation of soil parameters for the forest region named “Forest 3”. Plots of the quantity δ_F given by (10) versus the real dielectric constant ϵ_{rg} and conductivity σ_g of a clayey soil; (a) 3D, (b) 2D, plot.

D.2. Estimation of electric properties of clayey soil in grasslands

The method described in Section IV-B is used to recover the electric properties of the ground soil of the grassland area named “Grass 1”, see Fig. 4, from the corresponding PolSAR data presented in Figs. 5 (b), (c), (d) with the ground truth shown in Fig. 5 (a).

The quantity δ_G , expressed in (15), is plotted as a function of ϵ_{rg} and σ_g in a three-dimensional plot as shown in Fig. 7. The ϵ - σ characteristic curve of the soil is also plotted in the $(\epsilon_{rg}-\sigma_g)$ plane of Fig. 7. It is shown that δ_G has a sharp minimum of 9×10^{-4} at the point $\epsilon_{rg} = 11.6$ and $\sigma_g = 0.181 S/m$, which almost lies on the ϵ - σ characteristic curve of the clayey soil as shown in Fig. 7, where the corresponding water content of the soil is 24.1%. The recovered values of the electric properties, ϵ_{rg} and σ_g , and the water content are listed in Table 4 with the resulting estimation errors. It is found that these errors are very small, which reflects the efficiency of the proposed method to estimate the soil parameters.

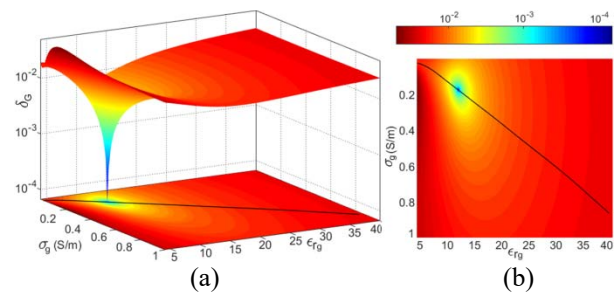


Fig. 7. Estimation of soil parameters for the grassland region named “Grass1”. Plots of the function δ_G given by (15) versus the real dielectric constant ϵ_{rg} and conductivity σ_g of a clayey soil; (a) 3D, (b) 2D, plot.

Table 4: The ground soil parameters used for generating the SAR data for the forested area named “Grassland 1”; see Table 2. The recovered values of these parameters using the proposed method and the resulting percentage estimation errors are listed in the last two rows of the table

Soil Parameter	Dielectric Constant	Conductivity (S/m)	Water Content
	ϵ_{rg}	σ_g	w
Ground Truth	12.10	0.186	25.0 %
Estimated	11.60	0.181	24.1 %
Percentage Error	4.1 %	2.7 %	3.6 %

D.3. Estimation of electric properties of clayey bare soil

The method described in Section IV-C is used to recover the electric properties of the ground soil of the area named “Bare Land 2”, see Fig. 4, from the corresponding PolSAR data presented in Figs. 5 (b), (c), (d) with the ground truth shown in Fig. 5 (a).

The quantity δ_S , expressed in (20), is plotted as a function of ϵ_{rg} and σ_g in a three-dimensional plot as shown in Fig. 8. The ϵ - σ characteristic curve of the soil is also plotted in the $(\epsilon_{rg}$ - σ_g) plane of Fig. 8. It is shown that δ_S has a sharp minimum of 9×10^{-4} at the point $\epsilon_{rg} = 35.4$ and $\sigma_g = 0.757$ S/m, which almost lies on the ϵ - σ characteristic curve of the clayey soil as shown in Fig. 8, where the corresponding water content of the soil is 56.0%. The recovered values of the electric properties, ϵ_{rg} and σ_g , and the water content are listed in Table 5 with the resulting estimation errors of the retrieved values. It is shown that the percentage errors are very small, which indicates the accuracy of the proposed method.

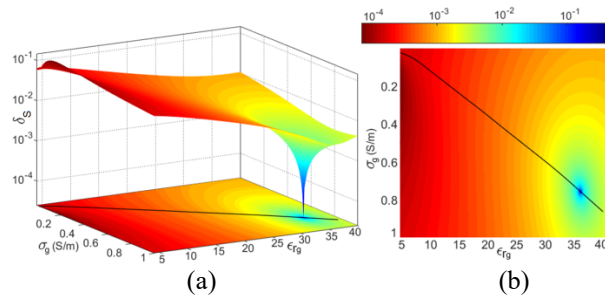


Fig. 8. Estimation of soil parameters for the bare land region named “Bare Land 2”. Plots of the function δ_S given by (20) versus the real dielectric constant ϵ_{rg} and conductivity σ_g of a clayey soil; (a) 3D, (b) 2D, plot.

VII. CONCLUSIONS

A new method is proposed to estimate the electric properties and water content of ground soil by apply-

Table 5: The ground soil parameters used for generating the SAR data for the forested area named “Bare Land 2”; see Table 2. The recovered values of these parameters using the proposed method and the resulting percentage error of the estimated values are listed in the last two rows of the table

Soil Parameter	Dielectric Constant	Conductivity (S/m)	Water Content
	ϵ_{rg}	σ_g	w
Ground Truth	35.40	0.759	56.0 %
Estimated	35.40	0.757	56.0 %
Percentage Error	0.0 %	0.26 %	0.0 %

ing the Target Decomposition (TD) theory for PolSAR images with the help of the ϵ - σ characteristic curves of the soil which are unique for each soil type at a specific frequency. This method is examined for the clayey type soil which is found in most naturally vegetated land areas. Also, a new method is developed based on the reverse of PolSAR TD theory, for realistic PolSAR images simulation of natural lands. Numerical results are presented for realistic PolSAR datasets using the proposed inverse TD theory method for Luxor city in Egypt. Also, numerical results are presented for quantitative assessment of the method proposed for the retrieval of the electric properties and water content of the clayey soil using the generated datasets. It is found, through the numerical investigations and quantitative assessment, that the dielectric constant, electric conductivity, and water content of the investigated clayey types of soil are accurately estimated.

APPENDIX

A.1. Covariance matrix for polarimetric SAR data

The reciprocity of backscattering of the radar pulse implies that $S_{hv} = S_{vh}$. Hence, the 3×3 -element covariance matrix of the data collected by the four-channel PolSAR system can be expressed as three-channel data as follows.

$$\begin{aligned} \Sigma &= [c_{11} \ c_{12} \ c_{13} \ c_{21} \ c_{22} \ c_{23} \ c_{31} \ c_{32} \ c_{33}] \\ &= \begin{bmatrix} \sigma_{hh}^2 & \sqrt{2}\sigma_{hh,hv}^2 & \sigma_{hh,vv}^2 \\ \sqrt{2}\sigma_{hh,hv}^2 & 2\sigma_{hv}^2 & \sqrt{2}\sigma_{hv,vv}^2 \\ \sigma_{hh,vv}^2 & \sqrt{2}\sigma_{hv,vv}^2 & \sigma_{vv}^2 \end{bmatrix}. \end{aligned} \quad (A.1)$$

The elements of the covariance matrix are the ensemble averages of the autocorrelation and cross-correlation of the scattering coefficients of the three channels [13]:

$$\begin{aligned} \Sigma &= \begin{bmatrix} |S_{hh}|^2 \hat{\zeta} & \sqrt{2}iS_{hh}S_{hv}^* \hat{\zeta} & iS_{hh}S_{vv}^* \hat{\zeta} \\ \sqrt{2}iS_{hh}S_{hv}^* \hat{\zeta} & 2|S_{hv}|^2 \hat{\zeta} & \sqrt{2}iS_{hv}S_{vv}^* \hat{\zeta} \\ iS_{hh}S_{vv}^* \hat{\zeta} & \sqrt{2}iS_{hv}S_{vv}^* \hat{\zeta} & |S_{vv}|^2 \hat{\zeta} \end{bmatrix}. \end{aligned} \quad (A.2)$$

The backscattered power for each of the three channels (HH, HV, VV) is given by main diagonal elements c_{11} , c_{22} , and c_{33} :

$$c_{11} = \sigma_{hh}^2, \quad c_{22} = 2\sigma_{hv}^2, \quad c_{33} = \sigma_{vv}^2. \quad (\text{A.3})$$

The total ratio of the backscattered power to the power illuminating the SAR target can be formulated as the sum of the main diagonal elements of Σ :

$$\sigma_p^2 = c_{11} + c_{22} + c_{33} = \sigma_{hh}^2 + 2\sigma_{hv}^2 + \sigma_{vv}^2. \quad (\text{A.4})$$

The correlation between the co-polarized and cross-polarized channels (HH, HV) and (HV, VV) is described by the elements c_{23} and c_{32} :

$$c_{12} = c_{21}^* = \sqrt{2}\sigma_{hh,hv}^2, \quad c_{23} = c_{32}^* = \sqrt{2}\sigma_{hv,vv}^2. \quad (\text{A.5})$$

The correlation between the co-polarized channels (HH, VV) is given by the elements c_{13} and c_{31} :

$$c_{13} = c_{31}^* = \sigma_{hh,vv}^2. \quad (\text{A.6})$$

A normalized covariance matrix $\hat{\Sigma}$ of the PolSAR data have unity ratio of the backscattered power. It can be obtained by dividing the elements of Σ by σ_p^2 expressed in (A.4):

$$\begin{aligned} \hat{\Sigma} &= \frac{1}{\sigma_p^2} \Sigma \\ &= \begin{bmatrix} \hat{\sigma}_{hh}^2 & \sqrt{2}\hat{\sigma}_{hh,hv}^2 & \hat{\sigma}_{hh,vv}^2 \\ \sqrt{2}\hat{\sigma}_{hh,hv}^2 & 2\hat{\sigma}_{hv}^2 & \sqrt{2}\hat{\sigma}_{hv,vv}^2 \\ \hat{\sigma}_{hh,vv}^2 & \sqrt{2}\hat{\sigma}_{hv,vv}^2 & \hat{\sigma}_{vv}^2 \end{bmatrix} \end{aligned} \quad (\text{A.7})$$

A.2. Elementary covariance matrices

The theory of PolSAR target decomposition using the MCSM can be applied to expand the covariance matrix of the PolSAR data collected during microwave imaging of land covers involving both natural and man-made constituents [15–17].

A.2.1. Covariance matrices of the PolSAR backscatter data for elementary types of natural ground covers

The matrices \hat{C}_s , \hat{C}_d , and \hat{C}_v are the normalized elementary covariance matrices characterizing the backscattering due to single bounce, double bounce, and volume (vegetation), respectively, which may constitute the natural ground covers and can be evaluated using the following approximate analytic expressions:

$$\hat{C}_s = \frac{1}{P_s} \begin{bmatrix} |\beta|^2 & 0 & \beta & 0 & 0 & \beta^* & 0 & 1 \end{bmatrix}, \quad P_s = 1 + |\beta|^2. \quad (\text{A.8-a})$$

$$\hat{C}_d = \frac{1}{P_d} \begin{bmatrix} |\alpha|^2 & 0 & \alpha & 0 & 0 & 0 & \alpha^* & 0 & 1 \end{bmatrix}, \quad P_d = 1 + |\alpha|^2. \quad (\text{A.8-b})$$

$$\hat{C}_v = \frac{1}{P_v} [1 \ 0 \ 1/3 \ 0 \ 2/3 \ 0 \ 1/3 \ 0 \ 1], \quad P_v = \frac{8}{3}, \quad (\text{A.8-c})$$

where α and β are defined as follows [17]:

$$\alpha = e^{j2(\gamma_h - \gamma_v)} \frac{\Gamma_{gh} \Gamma_{gv}}{\Gamma_{wh} \Gamma_{wv}}, \quad (\text{A.9})$$

where Γ_{gh} and Γ_{gv} are the horizontal and vertical Fresnel reflection coefficients of the ground surface. Similarly, Γ_{wh} and Γ_{wv} are Fresnel reflection coefficients of the horizontal and vertical wall surface. The symbols γ_h and γ_v denote the phase attenuation of the horizontal and vertical electromagnetic waves, respectively.

β is the ratio of the HH backscatter to the VV backscatter of the single-bounce scattering model:

$$\beta = \frac{S_{hh}}{S_{vv}}. \quad (\text{A.10-a})$$

In the first-order Bragg surface case β is defined as:

$$\beta = \frac{\Gamma_h}{\Gamma_v}, \quad (\text{A.10-b})$$

where,

$$\Gamma_h = \frac{\cos\theta_i \cos\theta_i - \sqrt{\epsilon_r - \theta_i}}{\cos\theta_i \cos\theta_i + \sqrt{\epsilon_r - \theta_i}}, \quad (\text{A.11-a})$$

$$\Gamma_v = \frac{(\epsilon_r - 1)[\theta_i - \epsilon_r(1 + \theta_i)]}{[\epsilon_r \cos\theta_i \cos\theta_i + \sqrt{\epsilon_r - \theta_i}]^2}, \quad (\text{A.11-b})$$

where θ_i and ϵ_r are the incidence angle and the dielectric constant of the surface, respectively.

A.2.2. Covariance matrices of the backscatter from Man-made structures

The matrices \hat{C}_h and \hat{C}_w are the elementary covariance matrices characterizing the helix (rotating) scattering mechanism and wire (edge) scattering mechanism, respectively, which are found in the man-made structures and can be evaluated using the following approximate analytic expressions [17]:

$$\begin{aligned} \hat{C}_h &= \frac{1}{4} \begin{bmatrix} 1 & j^u \sqrt{2} & -1 & -j^u \sqrt{2} & 2 & j^u \sqrt{2} & -1 & -j^u \sqrt{2} & 1 \end{bmatrix}, \\ u &= \{1, \quad \text{for right helix} \quad -1, \quad \text{for left helix} \}. \end{aligned} \quad (\text{A.12-a})$$

$$\begin{aligned} \hat{C}_w &= \frac{1}{1 + |\gamma|^2 + 2|\rho|^2} \begin{bmatrix} |\gamma|^2 & \sqrt{2}\gamma\rho^* & \gamma & \sqrt{2}\gamma^*\rho & 2|\rho|^2 \\ \sqrt{2}\gamma^*\rho & \sqrt{2}\rho^* & 1 \end{bmatrix}, \quad \gamma = \frac{S_{hh}}{S_{vv}}, \quad \rho = \frac{S_{hv}}{S_{vv}}. \end{aligned} \quad (\text{A.12-b})$$

REFERENCES

- [1] F. Visconti and J. M. de Paz, "Electrical conductivity measurements in agriculture: the assessment of soil salinity," Chapter 5, *New Trends and Developments in Metrology*, Intech Open, 2016.
- [2] F. Lombardi, M. Lualdi, F. Picetti, P. Bestagini, G. Janszen, and L. A. D. Landro, "Ballistic ground penetrating radar equipment for blast-exposed security applications," *MDPI Remote Sensing*, vol. 12, 2020.
- [3] A. Al-Yaari, J. P. Wigneron, A. Ducharne, Y. H. Kerr, W. Wagner, G. D. Lannoy, R. Reichle, A. Al Bitar, W. Dorigo, P. Richaume, and A. Milon, "Global-scale comparison of passive (SMOS)

- and active (ASCAT) satellite based microwave soil moisture retrievals with soil moisture simulations (MERRA-Land)," *Remote Sensing of Environment*, pp. 614-626, 2014.
- [4] W. Zhao and Z. L. Li, "Sensitivity study of soil moisture on the temporal evolution of surface temperature over bare surfaces," *International Journal of Remote Sensing*, vol. 34, pp. 3314-3331, 2013.
- [5] K. Das and P. K. Paul, "Present status of soil moisture estimation by microwave remote sensing," *Journal of Cogent Geoscience*, vol. 1, 2015.
- [6] R. T. Gharechelou, J. T. S. Sumantyo, and B. A. Johnson, "Soil moisture retrieval using polarimetric SAR data and experimental observations in an arid environment," *ISPRS International Journal of Geo-Information*, vol. 10, no. 10, pp. 711, 2021.
- [7] J. Á. Mozos, J. Casalí, M. G. Audicana, and N. E. C. Verhoest, "Correlation between ground measured soil moisture and RADARSAT-1 derived backscattering coefficient over an agricultural catchment of Navarre (north of Spain)," *Journal of Biosystems Engineering*, vol. 92, no. 1, pp. 119-133, Sep. 2005.
- [8] G. Bertoldi, S. D. Chiesa, C. Notarnicola, L. Passolli, G. Niedrist, and U. Tappeiner, "Estimation of soil moisture patterns in mountain grasslands by means of SAR RADARSAT2 images and hydrological modeling," *Journal of Hydrology*, vol. 516, pp. 245-257, 2014.
- [9] S. A. M. Soliman, K. F. A. Hussein, and A. A. Ammar, "Electromagnetic simulation for estimation of forest vertical structure using PolSAR data," *Progress in Electromagnetics Research B (PIER B)*, vol. 90, pp. 129-150, 2021.
- [10] D. Poreh, A. Iodice, A. Natale, and D. Riccio, "Software tool for soil surface parameters retrieval from fully polarimetric remotely sensed SAR data," *Sensors*, vol. 20, no. 18, pp. 1-20, 2020.
- [11] V. Turkar and Y. S. Rao, "Effect of different target decomposition techniques on classification accuracy for polarimetric SAR data," *Technology Systems and Management Communications in Computer and Information Science*, vol. 145, pp. 138-145, 2011.
- [12] M. Riahi and A. Tavangar, "Prognosis of the effects of soil characteristics on the performance of landmine detection in ground-penetrating radar system—a case study," *2nd International Conf. on Technical Inspection and NDT*, 2008.
- [13] L. Zhang, B. Zou, H. Cai, and Y. Zhang, "Multiple-component scattering model for polarimetric SAR image decomposition," *IEEE Geoscience and Remote Sensing Letters*, vol. 5, no. 4, pp. 603-607, 2008.
- [14] A. Mavrovic, A. Roy, A. Royer, B. Filali, F. Boone, C. Pappas, and O. Sonnentag, "Dielectric characterization of vegetation at L band using an open-ended coaxial probe," *Geosci. Instrum. Method. Data Syst.*, vol. 7, pp. 195-208, 2018.
- [15] Y. Yamaguchi, A. Sato, W.-M. Boerner, R. Sato, and H. Yamada, "Four-component scattering power decomposition with rotation of coherency matrix," *IEEE Trans. Geosci. Remote Sens.*, vol. 49, no. 6, pp. 2251-2258, 2011.
- [16] A. Freeman and S. L. Durden, "A three-component scattering model for polarimetric SAR data," *IEEE Trans. Geosci. Remote Sens.*, vol. 36, no. 3, pp. 693-973, May 1998.
- [17] L. Zhang, B. Zou, H. Cai, and Y. Zhang, "Multiple-component scattering model for polarimetric SAR image decomposition," *IEEE Geoscience and Remote Sensing Letters*, vol. 5, no. 4, 2008.



Mai Z. Ibrahim was born in El-Sharqia, Egypt. She received her B.Sc. in Electronics and Electrical Communication Engineering from the Higher Institute of Engineering in Belbeis in May 2018. She is working currently toward an M.Sc in Synthetic Aperture Radar Image Processing for the Classification of Land Covers at the Faculty of Electronic Engineering, Menoufia University. Her area of research involves radar imaging techniques, remote sensing, and electromagnetic wave propagation.



Ahmed I. M. Bahnacy received his B.Sc. in Radio Communication Engineering, Faculty of Electronic Engineering, Menouf, Egypt, in May 1981. He received an M.Sc degree in Electrical Communications (Antennas), from the Faculty of Engineering, Cairo University, Cairo, Egypt, Nov. 1987. Ph.D. in Electrical Communications (Antennas), Faculty of Electronic Engineering, Menouf, Egypt, in 1993, in collaboration with Robert Gordon Institute of Technology (RGIT), Aberdeen, UK. Lecturer, Dept. of Electronics & Electrical Communications, Faculty of Electronic Engineering, Menouf, 32952, Egypt from 1993-2000. Assoc. Prof., Dept. of Electronics & Electrical Communications, Faculty of Electronic Engineering, Menouf 32952, Egypt since Dec. 2000. From 2001 to 2011, he was with the College of Technology in Tabouk, Saudi Arabia. He went back to his position in Egypt in 2011. In 2018 he became an Emeritus Professor in the same Department.



Khalid F. A. Hussein received his B.Sc., M.Sc., and Ph.D. degrees from the Department of Electronics and Electrical Communications, Faculty of Engineering, Cairo University, in 1990, 1995, and 2001, respectively. He is currently a professor at the Department of

Microwave Engineering at the Electronics Research Institute. He has more than 29 years of research experience and more than 20 years of teaching experience in engineering colleges at various universities. He has supervised more than seventy doctoral and master theses. He has published more than 100 papers in international, regional, and local scientific journals and conferences. He has served as Head of the Microwave Engineering Department at the Electronics Research Institute for four years. He has been a member of the Egyptian Space Program (currently the Egyptian Space Agency) for more than eight years. He has worked as Principal Investigator for four research projects and Head of Research Group in four other research projects. He designed and implemented several satellite antennas from prototypes to finished products. He has provided scientific consultations and conducted field measurements related to the design and distribution of mobile communication base station antennas for good signal coverage on behalf of many Egyptian and international companies. His research interests include antennas, electromagnetic wave propagation, risk assessment of human exposure to microwave radiation, optical communications, photonics, quantum computing, radar systems, particularly ground penetrating radar (GPR), synthetic aperture radar (SAR), and remote sensing systems.



Asmaa E. Farahat received her B.Sc. and M.Sc. from the Department of Biomedical Engineering, Faculty of Engineering, Cairo University, in 2002 and 2006, respectively. She received her Ph.D. in 2012 from Ain Shams University. She is currently an Associate Professor at the Department of Microwave Engineering at the Electronics Research Institute. She has approximately 17 years of research experience. She has published more than 35 papers in international, regional, and local scientific journals and conferences. She has worked as a secondary investigator for three research projects. Her research interests include antennas, electromagnetic wave propagation, risk assessment of human exposure to microwave radiation, remote sensing systems, and radars.

Her research interests include antennas, electromagnetic wave propagation, risk assessment of human exposure to microwave radiation, remote sensing systems, and radars.